Structural Engineering and Mechanics, *Vol. 64, No. 4 (2017) 473-485*
DOI: https://doi.org/10.12989/sem.2017.64.4.473

Response spectrum analysis considering non-classical damping in the base-isolated benchmark building

Huating Chen*, Ping Tan[a], Haitao Ma[a] and Fulin Zhou[a]

Earthquake Engineering Research & Test Center, Guangzhou University, Guangzhou, China

(Received August 1, 2016, Revised June 29, 2017, Accepted August 4, 2017)

Abstract. An isolated building, composed of superstructure and isolation system which have very different damping properties, is typically non-classical damping system. This results in inapplicability of traditional response spectrum method for isolated buildings. A multidimensional response spectrum method based on complex mode superposition is herein introduced, which properly takes into account the non-classical damping feature in the structure and a new method is developed to estimate velocity spectra from the commonly used displacement or pseudo-acceleration spectra based on random vibration theory. The error of forced decoupling method, an approximated approach, is discussed in the viewpoint of energy transfer. From the base-isolated benchmark model, as a numerical example, application of the procedure is illustrated companying with comparison study of time-history method, forced decoupling method and the proposed method. The results show that the proposed method is valid, while forced decoupling approach can't reflect the characteristics of isolated buildings and may lead to insecurity of structures.

Keywords: response spectrum method; CCQC rule; complex mode superposition approach; forced decoupling method; velocity response spectra; the base-isolated benchmark building

1. Introduction

Isolated buildings, including heavy damping isolation system and light damping superstructure, are typical non-classically damped systems. Various methods have been developed to assess the peak responses for non-classically damped systems using response spectrum methods (Singh 1980, Igusa and Kiureghian 1983, Gupta and Jaw 1986, Villaverde 1988, Yang *et al*. 1990, Sinha and Igusa 1995, Zhou *et al*. 2004). There is also an approximate and commonly used approach which ignores the off-diagonal elements of damping matrix in undamped modal space so that the classical response method, CQC combination rule (Kiureghian 1981) can still be applied. Due to the characteristic, it is known as forced decoupling method (FDM) (Cronin 1976). When the degree of non-classical property is heavy, FDM may lead to significant errors (Warburton and Soni 1977). For isolated buildings, Tsai and Kelly (1988) considered that the response of base-isolated structures can be determined by FDM to some degree of accuracy. However, their results were based on the 10 percent damping ratio of the isolation system. In fact, when the damping ratio of isolation system increase to 20 percent which is a common damping level, the error of FDM becomes significant as illustrated in this paper.

The base-isolated benchmark model developed by ASCE, Gavin and Johnson (2006) firstly provide systematic and standardized means by which different analysis methods can be evaluated. This model is the University of Southern California Teaching Hospital, an existing building in Los Angeles, California. In this paper the benchmark model is used as a numerical example, which is more representative to evaluate the effectiveness of different analysis procedures.

Considering the features of isolated buildings, a response spectrum method suitable for isolated structures is derived in this paper. The combination rule taking multidimensional input excitations into account is based on complex complete quadratic combination (CCQC) proposed by Zhou *et al*. (2004). Due to the non-classical damping, relative velocity spectra are introduced. Unlike some investigators aforementioned who replace velocity spectra by pseudo-velocity spectra, which may lead to large errors for long period structures, especially for isolated buildings with heavy damped isolation system, a new method is developed to estimate velocity spectra from the commonly used displacement spectra or pseudo acceleration spectra based on random vibration theory. Thereafter, the errors of FDM are discussed from the energy viewpoint. As a numerical example, the base-isolated benchmark model aforementioned is presented to illustrate the application of the rule, and a comparative study with time history solutions as exact results and FDM are performed to demonstrate their validity and accuracy.

2. Equations of motion

Isolated buildings can be divided into superstructure and isolation system as shown in Fig. 1. Let $\mathbf{M}_s$, $\mathbf{C}_s$ and $\mathbf{K}_s$

*Corresponding author, Ph.D.
E-mail: sdcht2008@yeah.net
[a]Professor

ISSN: 1225-4568 (Print), 1598-6217 (Online)

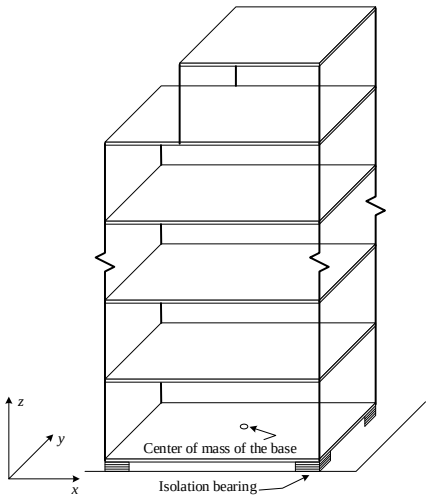

Fig. 1 A base-isolated structure in three-dimensional space

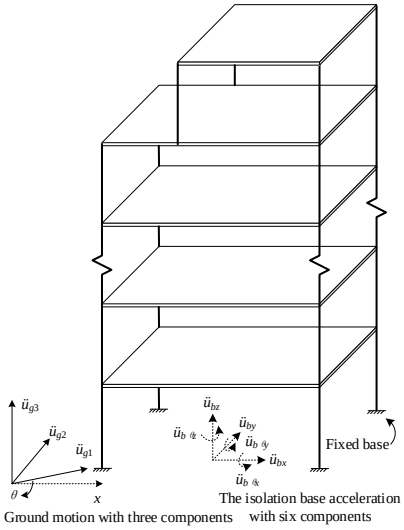

Fig. 2 The superstructure subjected to ground excitation and the acceleration of the isolation base

represent mass matrix, damping matrix and stiffness matrix of the superstructure in fixed-base, respectively. It is worth to note that $\mathbf{C}_s$ is a classical damping matrix. Since the isolation slab is so rigid that all isolation bearings can deform uniformly, the isolation system can be modeled by an equivalent element at the center of mass of the base.

It is convenient to work with relative displacements of the superstructure respect to the isolation base. The superstructure is subjected to the ground motion and the acceleration of the isolation base as shown in Fig. 2.

Considering three-component ground excitation, the dynamic equations of the superstructure can be written as

$$\mathbf{M}_s\ddot{\mathbf{u}}_s + \mathbf{C}_s\dot{\mathbf{u}}_s + \mathbf{K}_s\mathbf{u}_s = -\mathbf{M}_s[\mathbf{R}_{s1}\mathbf{T}\ddot{\mathbf{u}}_g(t) + \mathbf{R}_{s2}\ddot{\mathbf{u}}_b(t)] \tag{1}$$

in which $\mathbf{u}_s$ and $\mathbf{u}_b(t)$ denote relative nodal displacements of the superstructure respect to the isolation base and relative nodal displacements of the isolation base respect to the ground, respectively. $\mathbf{R}_{s1}$ and $\mathbf{R}_{s2}$ are influence matrix of the seismic input such that their *k*th column couples the degrees of freedom of the superstructure to the corresponding *k*th ground and the isolation base motion component, respectively (refer to the Appendix A for more details). $\ddot{\mathbf{u}}_g(t) = [\ddot{u}_{g1}(t)\ \ddot{u}_{g2}(t)\ \ddot{u}_{g3}(t)]^{\mathrm{T}}$ is the input acceleration with horizontal component $\ddot{u}_{g1}(t)$ and $\ddot{u}_{g2}(t)$ and vertical component $\ddot{u}_{g3}(t)$. $\mathbf{T}$ represents the transformation matrix accounting for the effect of input angle θ, which can be expressed as

$$\mathbf{T} = \begin{bmatrix} \cos\theta & \sin\theta & 0 \\ -\sin\theta & \cos\theta & 0 \\ 0 & 0 & 1 \end{bmatrix} \tag{2}$$

Based on the Eq. (1), the inertia force vector of the superstructure is $\mathbf{f}_s = \mathbf{M}_s[\ddot{\mathbf{u}}_s + \mathbf{R}_{s1}\mathbf{T}\ddot{\mathbf{u}}_g(t) + \mathbf{R}_{s2}\ddot{\mathbf{u}}_b(t)]$. Then, the forces on the isolation base coming from the superstructure can be represented by $\mathbf{R}_{s2}^{\mathrm{T}}\mathbf{f}_s$. The dynamic equations of isolation base with mass matrix $\mathbf{M}_b$, damping matrix $\mathbf{C}_b$ and stiffness matrix $\mathbf{K}_b$, thus, can be given by

$$\begin{aligned} &\mathbf{R}_{s2}^{\mathrm{T}}\mathbf{M}_s\ddot{\mathbf{u}}_s + (\mathbf{R}_{s2}^{\mathrm{T}}\mathbf{M}_s\mathbf{R}_{s2} + \mathbf{M}_b)\ddot{\mathbf{u}}_b + \mathbf{C}_b\dot{\mathbf{u}}_b + \mathbf{K}_b\mathbf{u}_b \\ &= -(\mathbf{R}_{s2}^{\mathrm{T}}\mathbf{M}_s\mathbf{R}_{s1} + \mathbf{M}_b\mathbf{R}_{s3})\mathbf{T}\ddot{\mathbf{u}}_g \end{aligned} \tag{3}$$

where $\mathbf{R}_{s3}$ represents influence matrix of isolation system (refer to the Appendix A for more details). As well known, relative displacement vector $\mathbf{u}_s$ can expressed in the form of undamped modes of the superstructure, that is $\mathbf{u}_s = \mathbf{\Phi}_s\mathbf{y}_s$, where $\mathbf{\Phi}_s$ is a matrix including the first n modes, $\mathbf{y}_s$ are modal coordinates. When $n << N_s$ (the total number of degrees of freedom in the superstructure), the size of Eq. (1) can be reduced to a large degree. Using $\mathbf{u}_s = \mathbf{\Phi}_s\mathbf{y}_s$, Eq. (1) becomes

$$\ddot{\mathbf{y}}_s + \tilde{\mathbf{C}}_s\dot{\mathbf{y}}_s + \tilde{\mathbf{K}}_s\mathbf{y}_s = -\mathbf{\Phi}_s^{\mathrm{T}}\mathbf{M}_s[\mathbf{R}_{s1}\mathbf{T}\ddot{\mathbf{u}}_g(t) + \mathbf{R}_{s2}\ddot{\mathbf{u}}_b(t)] \tag{4}$$

where $\tilde{\mathbf{C}}_s = \mathrm{diag}(2\xi_i\omega_i)$, $\tilde{\mathbf{K}}_s = \mathrm{diag}(\omega_i^2)$, i=1,…,n, ω_i and ξ_i are the natural frequencies and viscous damping ratios of the superstructure, respectively. Eqs. (4)-(3) can be combined to represent the overall equations of motion for whole isolated structure, as follows

$$\mathbf{M}^*\ddot{\mathbf{u}}^* + \mathbf{C}^*\dot{\mathbf{u}}^* + \mathbf{K}^*\mathbf{u}^* = -\mathbf{R}^*\mathbf{T}\ddot{\mathbf{u}}_g \tag{5}$$

where

$$\mathbf{M}^* = \begin{bmatrix} \mathbf{I}_{n\times n} & \mathbf{\Phi}_s^{\mathrm{T}}\mathbf{M}_s\mathbf{R}_{s2} \\ \mathbf{R}_{s2}^{\mathrm{T}}\mathbf{M}_s\mathbf{\Phi}_s & \mathbf{R}_{s2}^{\mathrm{T}}\mathbf{M}_s\mathbf{R}_{s2} + \mathbf{M}_b \end{bmatrix} \quad \mathbf{C}^* = \begin{bmatrix} \tilde{\mathbf{C}}_s & \\ & \mathbf{C}_b \end{bmatrix}$$

$$\mathbf{K}^* = \begin{bmatrix} \tilde{\mathbf{K}}_s & \\ & \mathbf{K}_b \end{bmatrix} \quad \mathbf{R}^* = \begin{bmatrix} \mathbf{\Phi}_s^{\mathrm{T}}\mathbf{M}_s\mathbf{R}_{s1} \\ \mathbf{R}_{s2}^{\mathrm{T}}\mathbf{M}_s\mathbf{R}_{s1} + \mathbf{M}_b\mathbf{R}_{s3} \end{bmatrix} \quad \ddot{\mathbf{u}}^* = \begin{Bmatrix} \mathbf{y}_s \\ \mathbf{u}_b \end{Bmatrix}$$

3. Complex mode superposition approach

Normally, $\mathbf{C}^*$ is a non-classically damped matrix. Considering the isolated structure still being a linear system, it is very economical to solve Eq. (5) using complex

superposition mode approach, in which Eq. (5) should be expressed in the form of state equations firstly, that is

$$\mathbf{A}\dot{\mathbf{v}} + \mathbf{B}\mathbf{v} = -\mathbf{E}\mathbf{T}\ddot{\mathbf{u}}_g \tag{6}$$

where

$$\mathbf{A} = \begin{bmatrix} \mathbf{0} & \mathbf{M}^* \\ \mathbf{M}^* & \mathbf{C}^* \end{bmatrix} \quad \mathbf{B} = \begin{bmatrix} -\mathbf{M}^* & \mathbf{0} \\ \mathbf{0} & \mathbf{K}^* \end{bmatrix}$$

$$\mathbf{E} = \begin{bmatrix} \mathbf{0} \\ \mathbf{R}^* \end{bmatrix} \qquad \mathbf{v} = \begin{Bmatrix} \dot{\mathbf{u}}^* \\ \mathbf{u}^* \end{Bmatrix}$$

The size of Eq. (6) becomes twice compared with Eq. (5), but it can be reduced by taking a small number of modes into account in Eq. (4). For non-classical damping systems, due to the non-positive definiteness of matrices **A** and **B**, the eigenvalue problem is complex-valued of order $2N_c$ (N_c denotes the total number of the unknown in Eq. (5)) and eigenvalues and eigenvectors occur in conjugate pairs. Let λ_i, $\boldsymbol{\psi}_i$, i=1,…$2N_c$, denote the eigenvalues and eigenvectors, respectively, and considering the definition of state vector **v**, eigenvector $\boldsymbol{\psi}_i$ is the form of $\boldsymbol{\psi}_i=[\lambda_i\boldsymbol{\phi}_i\ \boldsymbol{\phi}_i]^{\mathrm{T}}$, wherein $\boldsymbol{\phi}_i$ represent mode shapes. Comparing with the case of classical damping, we obtain $\lambda_i = -\xi_i\omega_i + \mathrm{i}\sqrt{1-\xi_i^2}\,\omega_i$. By complex mode superposition approach, the vector $\mathbf{u}^*$ can be expressed as

$$\mathbf{u}^*(t) = \sum_{i=1}^{N_c}[\boldsymbol{\phi}_i\boldsymbol{\eta}_i\mathbf{T}\mathbf{z}_i(t) + \bar{\boldsymbol{\phi}}_i\bar{\boldsymbol{\eta}}_i\mathbf{T}\bar{\mathbf{z}}_i(t)] \tag{7}$$

where $\mathbf{z}_i(t)$ are modal coordinates and can be obtained by

$$\dot{\mathbf{z}}_i(t) - \lambda_i\mathbf{z}_i(t) = -\ddot{\mathbf{u}}_g(t) \tag{8}$$

and $\boldsymbol{\eta}_i = \boldsymbol{\phi}_i^{\mathrm{T}}\mathbf{E}/(2\lambda_i\boldsymbol{\phi}_i^{\mathrm{T}}\mathbf{M}\boldsymbol{\phi}_i + \boldsymbol{\phi}_i^{\mathrm{T}}\mathbf{C}\boldsymbol{\phi}_i)$ denote modal participation factors. Notes that Eq. (4) are first-order differential equations and can be solved by classical mathematical methods.

It is more helpful to associate $\mathbf{z}_i(t)$ with dynamic equations of the normalized single degree of freedom (SDOF) systems

$$\ddot{\mathbf{q}}_i(t) + 2\xi_i\omega_i\dot{\mathbf{q}}_i(t) + \omega_i^2\mathbf{q}_i(t) = -\ddot{\mathbf{u}}_g(t) \tag{9}$$

in which ξ_i and ω_i denote the modal damping ratios and undamped natural frequencies, respectively. They can be obtained by $\omega_i = |\lambda_i|$, $\xi_i = -\mathrm{Re}(\lambda_i)/|\lambda_i|$. Through the derivative of the Duhamel integral, $\mathbf{z}_i(t)$ can be expressed in terms of $\mathbf{q}_i(t)$ and $\dot{\mathbf{q}}_i(t)$. That is

$$\mathbf{z}_i(t) = \dot{\mathbf{q}}_i(t) + (\xi_i\omega_i + \mathrm{i}\omega_{Di})\mathbf{q}_i(t) \tag{10}$$

where $\omega_{Di} = \sqrt{1-\xi_i^2}\,\omega_i$ are damped natural frequencies. Now substituting Eq. (6) into Eq. (3) will yield

$$\mathbf{u}^*(t) = \sum_{i=1}^{N_c}[\boldsymbol{\rho}_i\mathbf{T}\dot{\mathbf{q}}_i(t) + \boldsymbol{\varphi}_i\mathbf{T}\mathbf{q}_i(t)] \tag{11}$$

where $\boldsymbol{\rho}_i = 2\,\mathrm{Re}(\boldsymbol{\phi}_i\boldsymbol{\eta}_i)$, $\boldsymbol{\varphi}_i = -2\,\mathrm{Re}(\bar{\lambda}_i\boldsymbol{\phi}_i\boldsymbol{\eta}_i)$. This formulation is simpler and suitable for random vibration analysis. The response of $\mathbf{q}_i(t)$ and $\dot{\mathbf{q}}_i(t)$ can be evaluated by well-known numerical method in the time domain. In order to gain the response of superstructure, it is still necessary to transform the modal displacements $\mathbf{y}_s$ into physical displacements $\mathbf{u}_s$ by undamped modal matrix $\boldsymbol{\Phi}_s$ of the superstructure.

$$\mathbf{u}(t) = \sum_{i=1}^{N_c}\mathbf{T}'[\boldsymbol{\rho}_i\mathbf{T}\dot{\mathbf{q}}_i(t) + \boldsymbol{\varphi}_i\mathbf{T}\mathbf{q}_i(t)] \tag{12}$$

where $\mathbf{u}(t) = [\mathbf{u}_s^{\mathrm{T}}(t)\ \ \mathbf{u}_b^{\mathrm{T}}(t)]^{\mathrm{T}}$, $\mathbf{T}' = \mathrm{diag}(\boldsymbol{\Phi}_s, \mathbf{I}_{N_b})$, N_b is the total number of degrees of freedom in the isolation system. Appendix B represents more details of the derivation for Eqs. (7)-(12). Generally, a generic response quantity of interest can be expressed as a linear combination of the displacement, $R(t)=\mathbf{v}^{\mathrm{T}}\mathbf{u}(t)$, where **v** is a response transfer vector which is a function of the geometry and physical properties of the structure. According to Eq. (12) the response becomes

$$R(t) = \sum_{i=1}^{N_c}[\boldsymbol{\alpha}_i\mathbf{T}\dot{\mathbf{q}}_i(t) + \boldsymbol{\beta}_i\mathbf{T}\mathbf{q}_i(t)] \tag{13}$$

in which $\boldsymbol{\alpha}_i = \mathbf{v}^{\mathrm{T}}\mathbf{T}'\boldsymbol{\rho}_i = [\alpha_i^{(1)}\ \alpha_i^{(2)}\ \alpha_i^{(3)}]$, $\boldsymbol{\beta}_i = \mathbf{v}^{\mathrm{T}}\mathbf{T}'\boldsymbol{\varphi}_i = [\beta_i^{(1)}\ \beta_i^{(2)}\ \beta_i^{(3)}]$. The effect of input direction is illustrated explicitly from Eq. (13).

4. Response spectrum method

Assume the ground motion $\ddot{\mathbf{u}}_g(t)$ is a stationary Gaussian process and with no loss of generality, let $\ddot{\mathbf{u}}_g(t)$ be a zero-mean process. Penzien and Watabe (1975) have shown that the principal axes of ground motion exist, along which the ground motion components can be considered as uncorrelated. So the power density spectrum function matrix of the ground motion $\ddot{\mathbf{u}}_g(t)$ can be gained easily as $\mathbf{S}_g(\omega) = \mathrm{diag}[S_{g1}(\omega), S_{g2}(\omega), S_{g3}(\omega)]$. It is well known that the response of a linear system subjected to zero-mean Gaussian input is also a zero-mean Gaussian process. Then, the power spectral density of response $R(t)$ can be given by

$$S_R(\omega) = \sum_{i=1}^{N_c}\sum_{j=1}^{N_c}\{\omega^2\boldsymbol{\alpha}_i\mathbf{S}_{ij}(\omega)\boldsymbol{\alpha}_j^{\mathrm{T}} + \boldsymbol{\beta}_i\mathbf{S}_{ij}(\omega)\boldsymbol{\beta}_j^{\mathrm{T}} + \mathrm{i}\omega[\boldsymbol{\beta}_i\mathbf{S}_{ij}(\omega)\boldsymbol{\alpha}_j^{\mathrm{T}} - \boldsymbol{\alpha}_i\mathbf{S}_{ij}(\omega)\boldsymbol{\beta}_j^{\mathrm{T}}]\} \tag{14}$$

where $\mathbf{S}_{ij}(\omega) = H_i(\omega)\bar{H}_j(\omega)\mathbf{T}\mathbf{S}_g(\omega)\mathbf{T}^{\mathrm{T}}$ is the cross-spectral density matrix of modal responses $\mathbf{q}_i(t)$ and $\mathbf{q}_j(t)$, and $H_i(\omega) = 1/(\omega_i^2 - \omega^2 + \mathrm{i}2\xi_i\omega_i\omega)$ denotes the complex frequency response function of displacement. It is noted that $S_R(\omega)$ is always real-valued due to the symmetry. In the calculation of maximum responses, mean square is the quantity of interest. Meanwhile, introduce modal cross-correlation coefficients $\boldsymbol{\rho}_{m,ij} = \boldsymbol{\sigma}_{m,ij}/\sqrt{\boldsymbol{\sigma}_{m,ii}^2\boldsymbol{\sigma}_{m,jj}^2}$, m=0,1,2, in which $\boldsymbol{\sigma}_{m,ij}^2 = \int_{-\infty}^{+\infty}(\mathrm{i}\omega)^m\mathbf{S}_{ij}(\omega)\mathrm{d}\omega$, and for the convenience of expression, $\boldsymbol{\rho}_{0,ij}$, $\boldsymbol{\rho}_{1,ij}$ and $\boldsymbol{\rho}_{2,ij}$ are replaced by $\boldsymbol{\rho}_{ij}^{dd}$, $\boldsymbol{\rho}_{ij}^{vd}$

and $(-\boldsymbol{\rho}_{ij}^{vv})$, respectively, where the superscripts "*d*" and "*v*" mean displacement and velocity. In fact these above coefficients reflect the cross-correlation characteristics between modal displacement and modal velocity. Then according to Eq. (14), the mean square of the response $R(t)$, σ_R^2 can be expressed in terms of standard deviations of modal responses, $\boldsymbol{\sigma}_{\dot{q}_i}$ and $\boldsymbol{\sigma}_{q_i}$, as

$$\sigma_R^2 = \sum_{i=1}^{N_c}\sum_{j=1}^{N_c}\left\{\boldsymbol{\alpha}_i\boldsymbol{\rho}_{ij}^{vv}\boldsymbol{\sigma}_{\dot{q}_i}\boldsymbol{\sigma}_{\dot{q}_j}\boldsymbol{\alpha}_j^{\mathrm{T}} + \boldsymbol{\beta}_i\boldsymbol{\rho}_{ij}^{dd}\boldsymbol{\sigma}_{q_i}\boldsymbol{\sigma}_{q_j}\boldsymbol{\beta}_j^{\mathrm{T}} + [\boldsymbol{\beta}_i\boldsymbol{\rho}_{ij}^{vd}\boldsymbol{\sigma}_{\dot{q}_i}\boldsymbol{\sigma}_{q_j}\boldsymbol{\alpha}_j^{\mathrm{T}} - \boldsymbol{\alpha}_i\boldsymbol{\rho}_{ij}^{vd}\boldsymbol{\sigma}_{\dot{q}_i}\boldsymbol{\sigma}_{q_j}\boldsymbol{\beta}_j^{\mathrm{T}}]\right\} \tag{15}$$

Since the power density spectra of the three ground motion components are different from each other, the cross-correlation coefficients are also different in the three input directions.

Let $R_{\max}$ and $D_k(\omega, \xi)$, $V_k(\omega, \xi)$ represent the mean value of the maximum absolute response $R(t)$, and $q_k(t)$, $\dot{q}_k(t)$ of an oscillator with frequency ω and damping ratio ξ, respectively and "*k*" means that these responses are about the ground motion component $\ddot{u}_{gk}(t)$. The function $D_k(\omega, \xi)$ and $V_k(\omega, \xi)$ for variable ω and ξ can be defined as the mean relative displacement and velocity response spectrum of $\ddot{u}_{gk}(t)$. Note that the peak value of a Gaussian stationary process over a specified duration can be expressed as the product of peak factor and its root mean square (Vanmarcke 1972). Meanwhile assume the seismic input as white noise process and the peak factor of response $R(t)$ being similar to modal response peak factors, as done by Kiureghian (1981). Therefore, the maximum absolute responses of a structure can be evaluated through its response spectrum. That is

$$R_{\max}^2 = \left(R_{1x}^2 + R_{2y}^2\right)\cos^2\theta + \left(R_{2x}^2 + R_{1y}^2\right)\sin^2\theta + 2\left(R_{1xy} - R_{2xy}\right)\sin\theta\cos\theta + R_3^2 \tag{16}$$

where

$$R_{kx}^2 = \sum_{i=1}^{N_c}\sum_{j=1}^{N_c}\left(\rho_{ij}^{vv}\alpha_i^{(1)}\alpha_j^{(1)}V_{ki}V_{kj} + 2\rho_{ij}^{vd}\alpha_i^{(1)}\beta_j^{(1)}D_{ki}V_{kj} + \rho_{ij}^{dd}\beta_i^{(1)}\beta_j^{(1)}D_{ki}D_{kj}\right)$$

$$R_{ky}^2 = \sum_{i=1}^{N_c}\sum_{j=1}^{N_c}\left(\rho_{ij}^{vv}\alpha_i^{(2)}\alpha_j^{(2)}V_{ki}V_{kj} + 2\rho_{ij}^{vd}\alpha_i^{(2)}\beta_j^{(2)}D_{ki}V_{kj} + \rho_{ij}^{dd}\beta_i^{(2)}\beta_j^{(2)}D_{ki}D_{kj}\right)$$

$$R_{kxy}^2 = \sum_{i=1}^{N_c}\sum_{j=1}^{N_c}\left[\rho_{ij}^{vv}\alpha_i^{(1)}\alpha_j^{(2)}V_{ki}V_{kj} + \rho_{ij}^{dd}\beta_i^{(1)}\beta_j^{(2)}D_{ki}D_{kj} + \rho_{ij}^{vd}\left(\alpha_i^{(1)}\beta_j^{(2)} + \alpha_i^{(2)}\beta_j^{(1)}\right)D_{ki}V_{kj}\right]$$

$$R_3^2 = \sum_{i=1}^{N_c}\sum_{j=1}^{N_c}\left(\rho_{ij}^{vv}\alpha_i^{(3)}\alpha_j^{(3)}V_{3i}V_{3j} + 2\rho_{ij}^{vd}\alpha_i^{(3)}\beta_j^{(3)}D_{3i}V_{3j} + \rho_{ij}^{dd}\beta_i^{(3)}\beta_j^{(3)}D_{3i}D_{3j}\right)$$

and R_{kx}, R_{ky} represent the maximum responses when the relative displacement spectra D_k and velocity spectra V_k in which "*k*" devotes ground motion component act along the structure reference *x* and *y*, respectively. R_{kxy} is a cross term between response R_{kx} and R_{ky}. Due to the assumption of white noise as input excitation, the cross-correlation coefficients have closed forms (Zhou *et al*. 2004) as follows ($r=\omega_i/\omega_j$)

$$\rho_{ij}^{vv} = \frac{8\sqrt{\xi_i\xi_j}(\xi_i + r\xi_j)r^{3/2}}{(1-r^2)^2 + 4\xi_i\xi_j r(1+r^2) + 4(\xi_i^2+\xi_j^2)r^2}$$

$$\rho_{ij}^{vd} = \frac{4\sqrt{\xi_i\xi_j}(1-r^2)r^{1/2}}{(1-r^2)^2 + 4\xi_i\xi_j r(1+r^2) + 4(\xi_i^2+\xi_j^2)r^2}$$

$$\rho_{ij}^{dd} = \frac{8\sqrt{\xi_i\xi_j}(r\xi_i + \xi_j)r^{3/2}}{(1-r^2)^2 + 4\xi_i\xi_j r(1+r^2) + 4(\xi_i^2+\xi_j^2)r^2}$$

Eq. (16) is the modal combination rule of multidimensional input excitations for non-classically damped systems. It should be noted that both relative velocity and displacement spectra exist in Eq. (16). In practice, the displacement or pseudo acceleration spectra are often known. For convenient expression, some researchers always replace relative velocity spectra by pseudo velocity spectra, which may result in significant errors in long period phase with high damping ratios.

5. Estimation of the relative velocity spectrum

As demonstrated in Eq. (16), relative velocity spectra are needed to evaluate the maximum seismic design responses of isolated buildings. A method is developed hereby to estimate relative velocity spectra from commonly used relative displacement spectra or pseudo acceleration spectra based on random vibration theory.

As well known, the maximum displacement and velocity of a SDOF system subjected to a Gaussian excitation can be expressed, respectively, as

$$D(\omega_n, \xi) = p_d\sqrt{\lambda_0} \qquad V(\omega_n, \xi) = p_v\sqrt{\lambda_2} \tag{17}$$

where $D(\omega_n, \xi)$ and $V(\omega_n, \xi)$ represent spectra displacement and spectra velocity, respectively. $\lambda_m = \int_0^{+\infty}\omega^m S_d(\omega)\mathrm{d}\omega$, m=0,2 are the spectral moments, in which $S_d(\omega)$ is the one-side power spectral density function of displacement process. p_d and p_v are peak factors and their expressions developed by Davenport (1964) are used in this paper for its simplicity, as follows

$$p = \sqrt{2\ln\nu_0\tau} + 0.5772/\sqrt{2\ln\nu_0\tau} \tag{18}$$

where τ is the observation time duration, $\nu_0 = \sqrt{\lambda_2/\lambda_0}/\pi$ is the mean zero-crossing rate. Note that the peak factor is a function of time duration τ, natural frequency ω_n and damping ratio ξ of a SDOF system.

Assuming ground motions to be Gaussian white noise processes, that is $S_{\ddot{u}_g}(\omega) = S_0$, where S_0 is a constant. The spectral moments $\lambda_0 = \pi S_0/(4\xi\omega_n^3)$, $\lambda_2 = \pi S_0/(4\xi\omega_n)$ can be obtained (Kiureghian 1980). Then the mean zero-crossing rate of displacement can be expressed by $\nu_{0d}=\omega_n/\pi$.

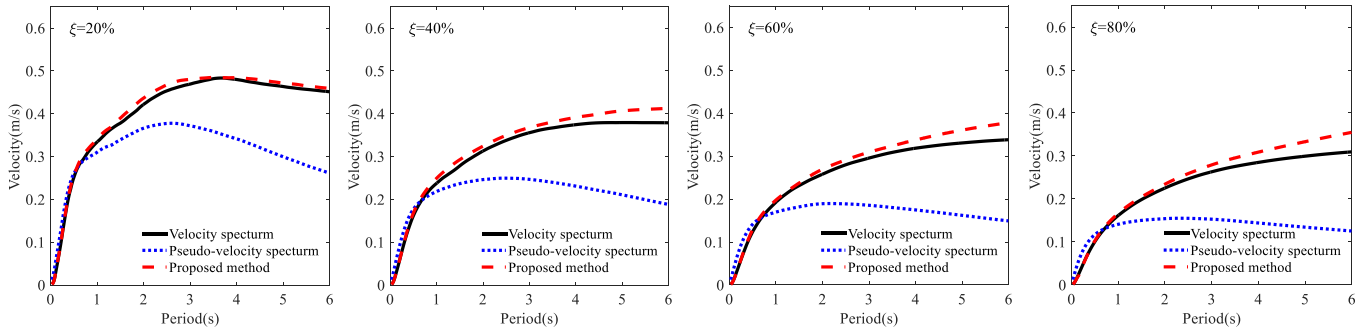

Fig. 3 Comparison of velocity spectra by exact values, pseudo velocity and new method for 20%, 40%, 60%, 80% damping ratios using artificial under artificial ground motions

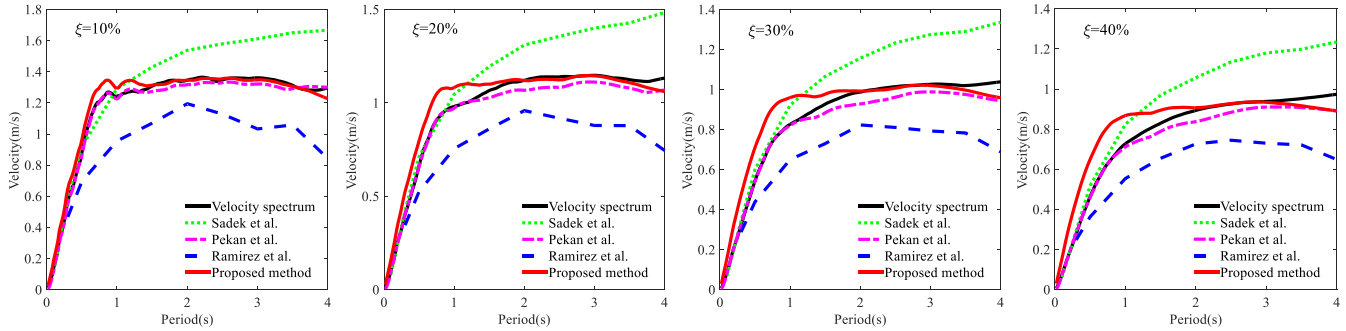

Fig. 4 Comparison of velocity spectra obtained by different methods for 10%, 20%,30% and 40% damping ratios under 28 near-field ground motions

So the displacement and velocity peak factors can be expressed explicitly, as

$$p_d(\omega_n,\tau)=\sqrt{2\ln(\omega_n\tau/\pi)}+0.5772/\sqrt{2\ln(\omega_n\tau/\pi)} \tag{19}$$

$$p_v(\omega_n,\tau)=\sqrt{2\ln\nu_{0v}\tau}+0.5772/\sqrt{2\ln\nu_{0v}\tau} \tag{20}$$

where ν_{0v} is associated with ω_n, ξ and cut-off frequency ω_e of the input white noise excitation. That is,

$$\nu_{0v}=\frac{2\sqrt{\omega_n[\xi\omega_e-\pi\omega_n(\xi^2-0.25)]}}{\pi^{3/2}}$$

From these formulation, we can observe that the displacement peak factor is independent of damping ratio ξ when the excitation is a white noise. Therefore, velocity spectrum can be expressed in terms of displacement response spectrum as follows

$$V(\omega_n,\xi)=\upsilon(\omega_n,\xi)\omega_n D(\omega_n,\xi)=\upsilon(\omega_n,\xi)V_p(\omega_n,\xi) \tag{21}$$

in which $\upsilon(\omega_n, \xi)=p_v/p_d$, the peak factors p_v and p_d are calculated via Eq. (19) and Eq. (20), respectively. $V_p(\omega_n, \xi)$ represents pseudo-velocity spectrum. The expression aforementioned also shows that the convention assuming velocity spectrum to be equal to the pseudo-velocity spectrum ignores the effect of peak factors.

To verify the efficiency of Eq. (21), 200 artificially generated filtered white noise processes with peak ground acceleration of 0.2 g are used. The filtered white noise excitations are generated through a modified Kanai-Tajimi power spectra model suggested by Clough and Penzien (1991)

$$S_{\ddot{u}_g}(\omega)=S_0\frac{\omega_g^4+4\xi_g^2\omega_g^2\omega^2}{(\omega_g^2-\omega^2)^2+4\xi_g^2\omega_g^2\omega^2}\cdot\frac{\omega^4}{(\omega_f^2-\omega^2)^2+4\xi_f^2\omega_f^2\omega^2} \tag{22}$$

in which is S_0 a scale factor, ω_g and ξ_g are the filter parameters representing the natural frequency and damping ratio of the soil layer, respectively, and ω_f, ξ_f are parameters of a second filter that is introduced to assure finite variance of the ground displacement. Now we consider the stiff soil site and set ω_g=15 rad/s, ω_f=1.5 rad/s, ξ_g=0.6 and ξ_f=0.6. The PSD scale factor S_0 is selected such as to produce a mean peak ground acceleration of 0.2g over the ensemble of records. The response spectrum consistent with the PSD model is obtained via response history analysis of 200 artificial ground motions. The comparisons, which are illustrated in Fig. 3, of velocity spectrum, pseudo-velocity spectrum and the proposed method Eq. (21) show the efficiency of the proposed method for all levels of damping.

Sadek *et al*. (1999), Pekan *et al*. (1999) and Ramirez *et al*. (2000) also developed similarly simple methods to estimate the relative velocity spectrum. However, different from the proposed method in this paper, these studies are based on the statistical analysis of a selected series of earthquake records. Comparisons among these methods are shown in Figs. 4 and 5. For the convenience of comparison, the periods are selected from 0 to 4 sec. and the damping ratios are 0.1, 0.2, 0.3 and 0.4. The earthquake records used are suggested by ATC (2008) with 28 near-field and 22 far-

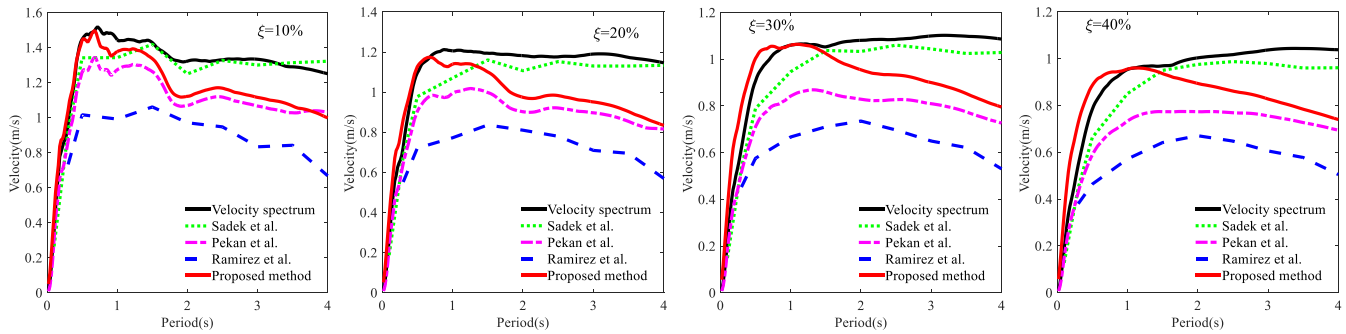

Fig. 5 Comparison of velocity spectra obtained by different methods for 10%, 20%,30% and 40% damping ratios under 22 far-field ground motions

field ground motions and each record is scaled such that the maximum ground velocity is 1 m/s in order to facilitate direct comparisons of results. From these two figures, it can be observed that the method developed by Pekan *et al*. has an excellent agreement with the actual velocity spectrum corresponding the 28 near-field ground motions while it does not work well for the far-field ground motions. This phenomenon can be easily understood because most of the utilized earthquake records in the study of Pekan *et al*. have near-fault characteristics. Instead, the method of Sadek *et al*. is more suitable for far-field ground motions. The proposed method also has good results for near-filed ground motions. On the other hand, for the far-filed ground motions, the proposed method is better than the methods developed by Pekan *et al*. and Ramirez *et al*.

6. Discussions of the forced decoupling method

Let **M**, **C** and **K** denote mass, damping and stiffness matrix of the whole isolated structure, respectively. For the convenience of expression, consider dynamic equations subjected to only one seismic component $\ddot{u}_g(t)$, which are described by

$$\mathbf{M}\ddot{\mathbf{u}}+\mathbf{C}\dot{\mathbf{u}}+\mathbf{K}\mathbf{u}=-\mathbf{M}\mathbf{r}\ddot{u}_g(t) \tag{23}$$

where **u** is the *N*-dimension vector of building displacements respect to ground motion and **r** represents the influence vector. It is obvious that **C** is non-classical damping matrix, and if **u** is expressed in term of undamped modes, **u**=**Φq**, Eq. (23) can be described by modal dynamic equations, as follows

$$\begin{aligned}&\ddot{q}_i(t)+2\xi_i\omega_i\dot{q}_i(t)+\omega_i^2 q_i(t)\\&=-\eta_i\ddot{u}_g(t)-\sum_{\substack{j=1\\j\neq i}}^{N}\mu_{ij}\dot{q}_j(t)\qquad i=1,...,N\end{aligned} \tag{24}$$

in which $q_i(t)$ is modal coordinate, ξ_i and ω_i denote damping ratio and natural frequency of the assumed classically damped system ignoring the last terms in the above equations, respectively. η_i is mode participation factor. $\mu_{ij}=\boldsymbol{\phi}_i^{\mathrm{T}}\mathbf{C}\boldsymbol{\phi}_j$ ($\boldsymbol{\phi}_i$ represents undamped mode vector) is the off-diagonal term of the transformed damping matrix and it is non-zero value for non-classical damping matrix. The equations above demonstrate that modal dynamic equations are coupled because of non-classical damping and energy transfer occurs among modal dynamic equations. So there are two functions of damping for non-classically damped systems, one plays a role of energy dissipation, coming from diagonal elements in the transformed damping matrix. The other is energy transfer resulting from off-diagonal terms. Using Fourier transformation, the frequency domain expressions of Eq. (24) can be described as

$$\begin{aligned}&[(\omega_i^2-\omega^2)+\mathrm{i}2\xi_i\omega_i\omega]Q_i(\omega)\\&=-\eta_i U_g(\omega)-\mathrm{i}\omega\sum_{\substack{j=1\\j\neq i}}^{N}\mu_{ij}Q_j(\omega)\end{aligned} \tag{25}$$

where $Q_i(\omega)$ and $U_g(\omega)$ are the Fourier transformations of $q_i(t)$ and $\ddot{u}_g(t)$, respectively. For isolated buildings, the responses are always dominated by the first modal response due to its larger modal participation factor η_1. Compared with the first modal velocity $\dot{q}_1(t)$, the other modal velocities $\dot{q}_j(t)$ are so small that they can be neglected in the first mode dynamic equation without introducing large errors. Note that the first mode mainly reflects characteristics of isolation system since the superstructure is very stiff as compared to the isolation system. Hence, using Eq. (25), the response of isolation base can expressed as (assume isolation base displacement in the mode vector being normalized)

$$Q_b(\omega)=-\frac{\eta_1 U_g(\omega)}{\omega_1^2-\omega^2+\mathrm{i}2\xi_1\omega_1\omega} \tag{26}$$

The first modal damping ratio ξ_1 is mainly contributed by the damping ratio of the isolation system, ξ_b (Kelly 1997). As can be seen, the displacement amplitude in Eq. (26) decreases with ξ_1 or ξ_b increasing. In addition, for other modal displacement amplitudes, recognizing that $\mu_{i1}Q_b(\omega)$ dominates in $\sum_{j=1}^{N}\mu_{ij}Q_j(\omega)$, $j\neq i$, the results can be simplified to

$$Q_i(\omega)=-\frac{\eta_i U_g(\omega)+\mathrm{i}\omega\mu_{i1}Q_b(\omega)}{\omega_i^2-\omega^2+\mathrm{i}2\xi_i\omega_i\omega}\quad i>1 \tag{27}$$

when ξ_b rises, which leads to both the coupling term μ_{i1} and modal damping ratios ξ_i increasing (Du *et al*. 2002),

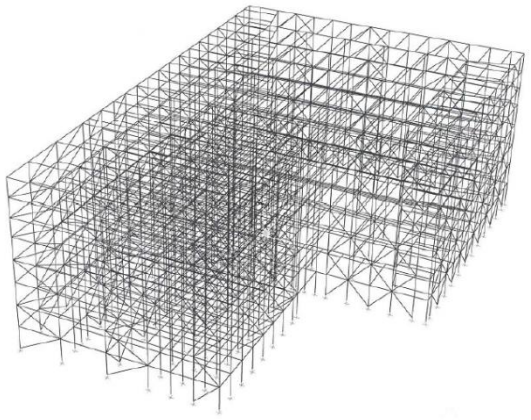

Fig. 6 Model of the superstructure

$Q_i(\omega)$ is dependent on their relative values. In fact, the energy dissipation part plays a major role with ξ_b increasing at first, then when ξ_b rises to a certain degree, the effect of energy transfer becomes significant as shown in the numerical example of the next section. This phenomena implies that optimum damping ratio ξ_b exists and beyond it the responses of superstructure begin to increase.

In FDM, the coupling terms due to non-classical damping are neglected, which implies that energy transfer among the modes is broken off. The modal responses are approximated by

$$Q_i(\omega) = -\frac{\eta_i U_g(\omega)}{\omega_i^2 - \omega^2 + \mathrm{i}2\xi_i\omega_i\omega} \quad i=1,...,N \tag{28}$$

The expression of responses in isolation base is consistent with Eq. (26), so FDM can predict displacement of isolation base exactly. The breaking of energy transfer has little effect on isolation system, while it impacts significantly responses of superstructure. Comparing Eq. (28) with Eq. (27), responses of superstructure in FDM are smaller than exact results. When the damping ratio of isolation system is light, little energy transfer occurs and the results by FDM can be accepted to some degree accuracy. However, with the level of non-classical damping increasing, the errors will increase as well. Since the only function of damping in the system is absorbing energy, the responses will decrease continually with ξ_b increasing as demonstrated in the numerical example in the next section. On the other hand, Hanson and Soon (2001) have tried to use the exact natural frequencies and modal damping ratios calculated by complex eigenvalue procedure to replace those in FDM in order to improve the accuracy of FDM, but the results are still disappointed. From the viewpoint of energy transfer, the errors of FDM come from the ignorance of influence among modal responses, which can interpret the results of Hanson and Soon.

7. Example application

The numerical example is the benchmark structure aforementioned, which is a base-isolated eight-story, steel-braced framed building with 82.4-m-long and 54.3-m-wide, as shown in Fig. 6. Floor slabs and the base are assumed to be rigid in plane. Therefore, the superstructure and the base can be modeled using three master degrees of freedom (DOF) including two horizontal displacements and one rotational displacement about vertical axis per floor at the center of mass. The combined model of the superstructure (24 DOFs) and isolation system (3 DOFs) consists of 27 degrees of freedom. All twenty four modes in the fixed-base case are employed to model the superstructure. The superstructure damping ratio of each mode is assumed to be 5%. The first three modal periods of the superstructure in the fixed-base are 0.89s, 0.78s and 0.66s, respectively.

The isolation system in the example is a linear isolation system consisting of 92 linear elastomeric bearings and a number of viscous dampers. The locations and numbers of these bearings are identical to those in the paper of Narasimhan *et al*. (2006).The stiffness applied herein of bearings are shown in Table 1, which guarantee stiffness eccentricities of the isolated structure as small as -8.08E-2m and 1.63E-2m in *x* and *y* directions, respectively. There are two approaches to calculate the modal properties. One is exact method, complex mode method and the other is approximate method, FDM. From Table 2 it can be seen that the non-classical damping has little influence on the modal properties. However, it doesn't imply that the non-classical damping has little influence on the structural responses as illustrated in the following section. As discussed above, the energy transfer due to non-classical damping from the isolation system to the superstructure may enlarge responses of the superstructure. The table also demonstrates that damping of isolation system has a significant contribution to modal damping ratios of the superstructure and the first three modes are mainly controlled by the isolation system.

Table 1 Stiffness of the elastomeric bearings

Stiffness (kN/m)	513	1026	1253	1396
Corresponding Number	17-25,54-61,79-87	1-3,26-31,50-53,62-64,88-92	32-49	4-16,65-78

Table 2 Modal properties of the benchmark isolated structure

Mode No.	Damping Ratio of Isolation System 20%				Damping Ratio of Isolation System 40%			
	Exact		FDM		Exact		FDM	
	ξ^* (%)	T^* (s)	ξ^* (%)	T^* (s)	ξ^* (%)	T^* (s)	ξ^* (%)	T^* (s)
1	18.87	3.14	18.98	3.17	36.68	3.05	37.89	3.17
2	18.82	2.99	18.74	3.00	37.89	2.93	37.41	3.00
3	21.71	2.61	21.48	2.61	45.58	2.65	42.89	2.61
4	12.17	0.56	12.10	0.56	17.42	0.56	17.08	0.56
5	11.20	0.49	11.14	0.49	15.66	0.49	15.30	0.49
6	11.52	0.43	11.47	0.43	16.13	0.43	15.91	0.43
7	9.35	0.22	9.30	0.22	11.74	0.22	11.56	0.22
8	8.31	0.21	8.28	0.21	10.06	0.21	9.98	0.21
9	8.42	0.17	8.39	0.17	10.24	0.17	10.16	0.17
10	6.97	0.14	6.96	0.14	7.85	0.14	7.84	0.14

*ξ and T denote modal damping ratios and modal periods, respectively.

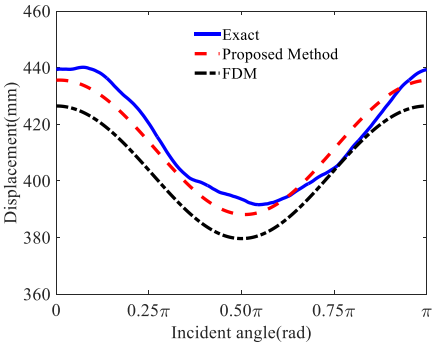

(a) *X* direction

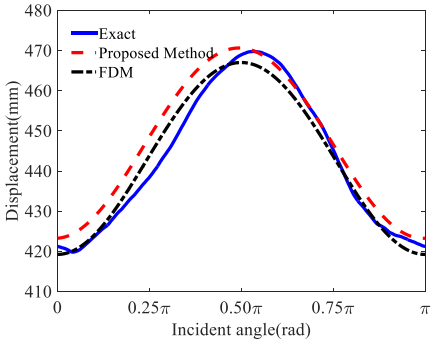

(b) *Y* direction

Fig. 7 Mean maximum displacements of the isolation base with different incident angle

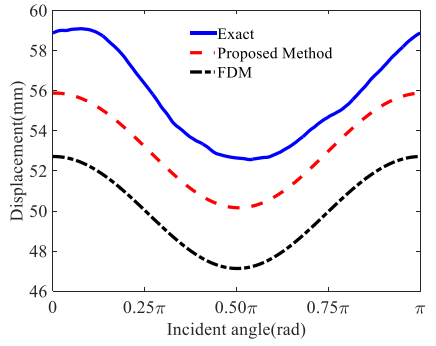

(a) *X* direction

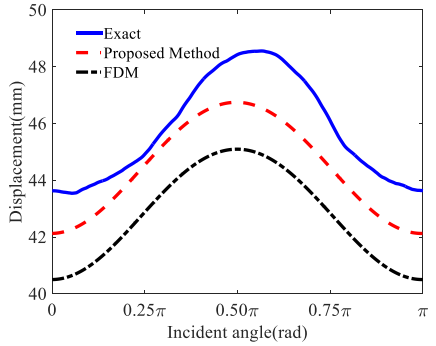

(b) *Y* direction

Fig. 8 Mean maximum displacements of the top story with different incident angle

Three methods are applied to compute the responses of the isolated structure. The first one is exact method which is time-history analysis approach using New-mark β integration. The second one is the proposed method in this paper which considers the effect of non-classical damping. The last one is forced decoupling method (FDM) based on classical damping assumption. 100 sets of filtered white noise processes with peak ground acceleration of 0.4 g are used as input excitations. Each set consists of two horizontal motions whose amplitude ratio is 0.85. The filtered white noise excitations are generated through the modified Kanai-Tajimi power spectra model described as Eq. (22). Figs. 7 and 8 show the comparison of exact method, FDM and the proposed method with the incident angles changing from 0 to π when the damping ratio of isolation system is 0.1. As can be seen, the proposed method is valid to some degree and the incident angle has little effect on accuracy of different methods. Both FDM and the proposed method can evaluate the maximum responses of isolation base well in all incident angles.

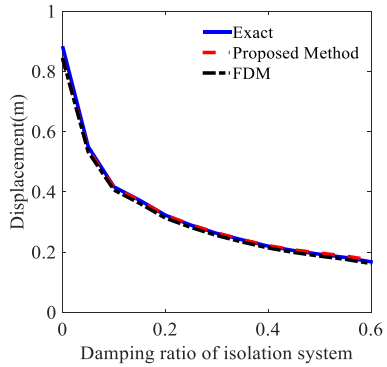

(a) *X* direction

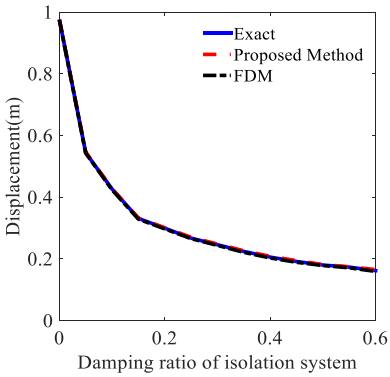

(b) *Y* direction

Fig. 9 Comparison of mean maximum displacements of the isolation base

The effect of damping level in the isolated system on the responses is studied and the damping ratio ξ_b is considered from 0 to 0.6. Fig. 9 shows that the mean maximum displacements of the isolation base have little differences between the proposed method and FDM respect to different damping levels of isolation system, which is consistent with the discussion aforementioned. However, for responses of the superstructure, when the damping ratio of isolation system is beyond 0.1, the differences between the proposed method and FDM become significant, and the proposed method is more accurate than FDM, as illustrated in Figs. 10 and 11. An interesting phenomenon can be observed that with the damping ratio of isolation system increasing, the displacement of the isolation base decreases all the time but

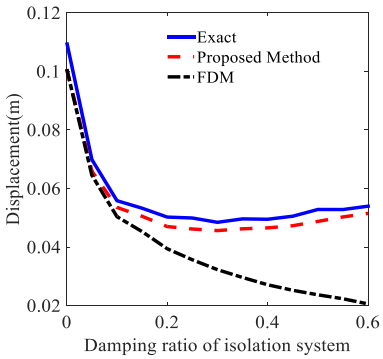

(a) *X* direction

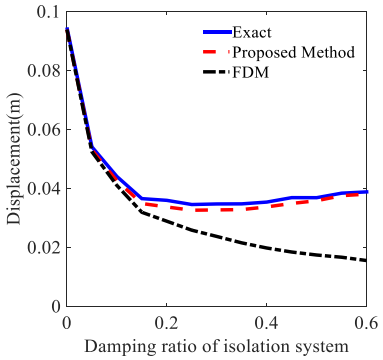

(b) *Y* direction

Fig. 10 Comparison of mean maximum displacements of the top story

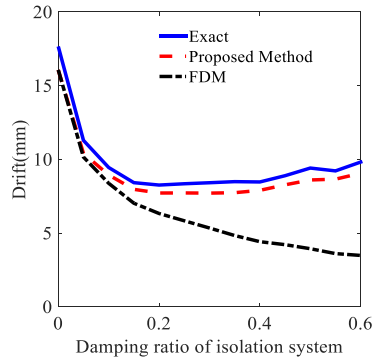

(a) *X* direction

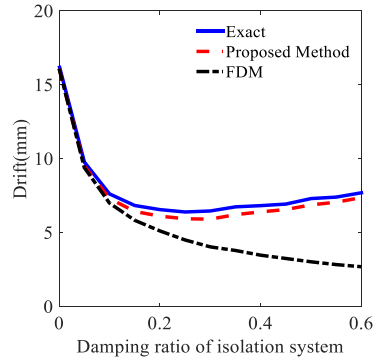

(b) *Y* direction

Fig. 11 Comparison of the mean maximum story drifts

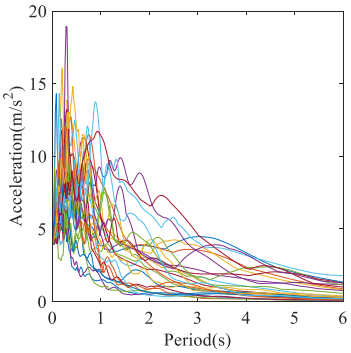

(a) *x* component

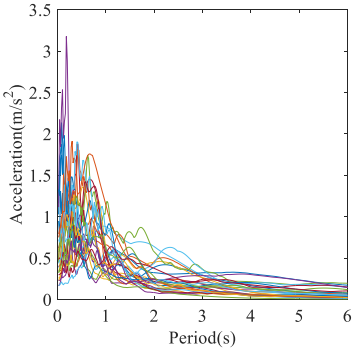

(b) *y* component

Fig. 12 The acceleration spectrum of 28 near-field ground motions for 5% damping ratio

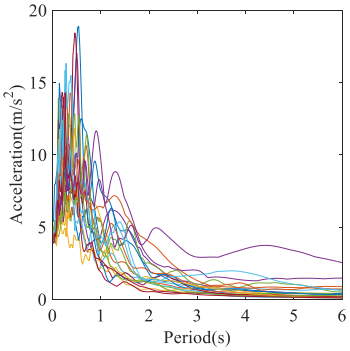

(a) *x* component

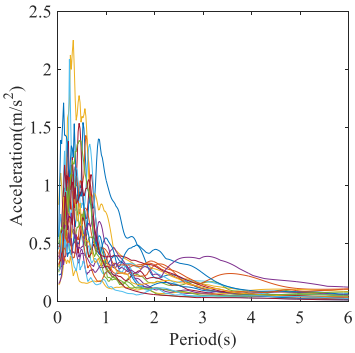

(b) *y* component

Fig. 13 The acceleration spectrum of 22 far-field ground motions for 5% damping ratio

the responses of the superstructure increase firstly then decrease, which is consistent with the study results of Kelly (1999). It implies that increasing damping of isolation system doesn't always decrease the responses of superstructure. It is noted that FDM approach doesn't reflect this characteristic. So in practice FDM approach may

mislead the design of isolation structures, which is easy to lead to insecurity of structures.

The results shown above are based on the artificial ground motions. As is well known, the characteristics of actual earthquake ground motion records are very complex. Therefore, it is necessary to validate the efficiency of the proposed method under real ground motion records. In this study, the aforementioned records, i.e., 28 sets of near-field and 22 sets of far-field ground motions suggested by ATC-63, are used and each set of records are scaled such that the maximum ground acceleration of one horizontal record, whose maximum ground acceleration is larger than the other one, is 0.4 g. Meanwhile, this horizontal record is named as *x* component and the other one is *y* component. Their acceleration spectrum corresponding 5% damping ratio are illustrated in Figs. 12 and 13. The same methods, i.e., time-history approach, the proposed method in this paper and FDM, are used in the dynamic analysis. The damping ratios of the isolation system arrange from 0 to 0.6 and the incident angles of all the excitation inputs are 0.

For the isolated structures, the response quantities of interest are the maximum displacement of the isolation base and the maximum story-drift of the superstructure. They are shown in Figs. 14-17. From these results, the same conclusions can be drawn that increasing the damping of the isolation system may amplify the responses of the superstructure and the proposed method in this paper also works well to predict the structural responses. It also can be observed that the error of FNM becomes larger under real ground motions especially for the superstructure.

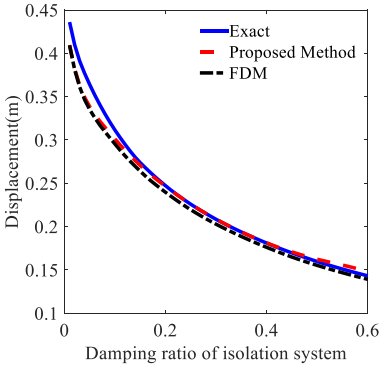

(a) *X* direction

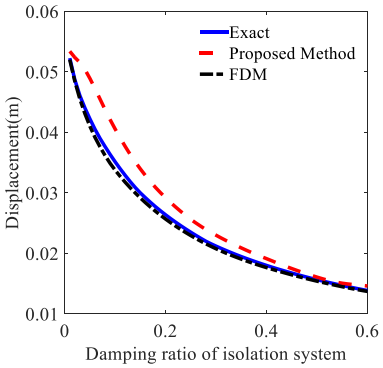

(b) *Y* direction

Fig. 14 Comparison of mean maximum displacements of the isolation base under 28 near-field ground motions

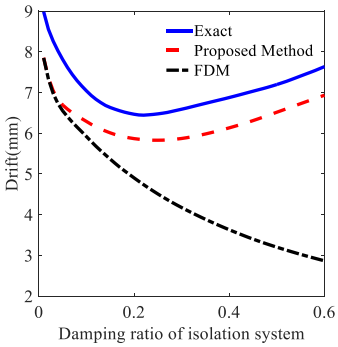

(a) *X* direction

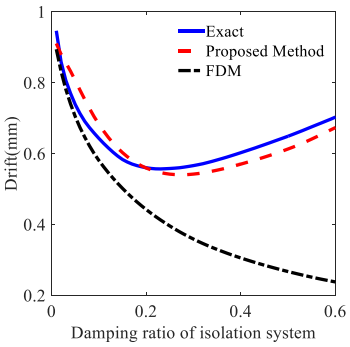

(b) *Y* direction

Fig. 15 Comparison of the mean maximum story drifts under 28 near-field ground motions

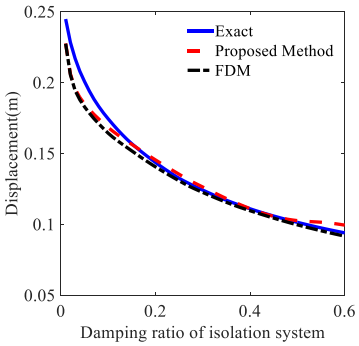

(a) *X* direction

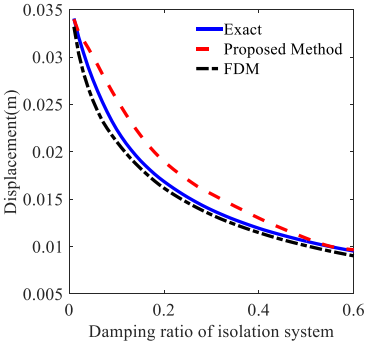

(b) *Y* direction

Fig. 16 Comparison of mean maximum displacements of the isolation base under 22 far-field ground motions

8. Conclusions

A rule has been established to combine peak modal responses of isolated structures, which can consider

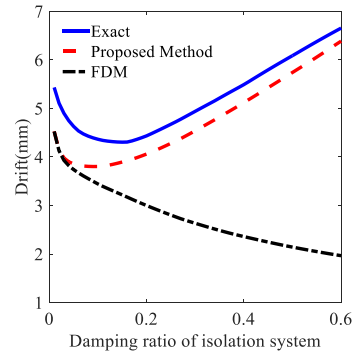

(a) *X* direction

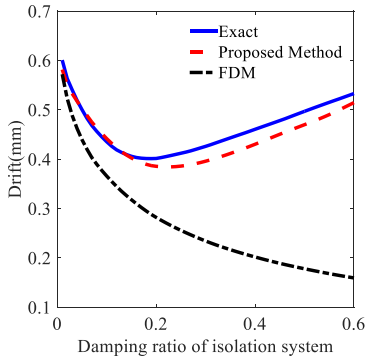

(b) *Y* direction

Fig. 17 Comparison of the mean maximum story drifts under 22 far-field ground motions

multidimensional seismic inputs. The derivation of the rule is based on random vibration theory, and its assumptions are similar to classical method (CQC). The only shortage is the computation of complex eigenvalues due to the two times size of structural matrices. But taking only the first small number of modes in the superstructure into account, which is reasonable for isolated structures, can reduce the computational scale significantly. A new method is developed to estimate velocity spectra from commonly used displacement spectra or pseudo acceleration spectra based on random vibration theory in this paper, which can evaluate the velocity spectra well at long periods and high damping ratios. The discussion of the error in FDM shows that non-classical damping mainly impacts the superstructure, which is helpful to interpret the numerical calculation results. The comparison of time history method, the proposed method in this paper and FDM based on the base-isolated benchmark model shows that all method are consistent in the predicting displacement of isolation base to some degree accuracy, however, FDM has remarkable errors when the damping ratio of isolation system is beyond 10 percent and the characteristic that the responses of the superstructure may increase with increasing of damping ratio of isolation system is not reflected by FDM.

Acknowledgments

This work was supported by the Program for Changjiang Scholars and Innovative Research Team in University under Grant No. IRT13057. The support is gratefully acknowledged.

References

ATC (2008), Quantification of Building Seismic Performance Factors, FEMA P695, ATC-63 Project Report; Applied Technology Council, Federal Emergency Management Agency, USA.

Clough, R.W. and Penzien, J. (1991), *Dynamics of Structures*, McGraw-Hill, New York, USA.

Cronin, DL. (1976), "Approximation for determining harmonically excited response of non-classically damped system", *J. Eng. Indust.*, **98**, 43-47.

Davenport, A.G. (1964), "Note on the distribution of the largest value of a random function with application to gust loading", *Proc. Inst. Civil Eng.*, **28**(2), 187-196.

Du, Y., Li, H. and Spencer, Jr. B.F. (2002), "Effect of non-proportional damping on seismic isolation", *J. Struct. Control*, **9**, 205-236.

Gupta, A.K. and Jaw, J.W. (1986), "Response spectrum method for non-classically damped systems", *Nucl. Eng. Des.*, **91**, 161-169.

Hanson, R.D. and Soong, T.T. (2001), "Seismic design with supplemental energy dissipation devices", EERI Monograph No. 8; Earthquake Engineering Research Institute, Oakland, CA.

Igusa, T. and Kiureghian, A.D. (1983), "Response spectrum method for systems with non-classical damping", *Proceeding of ASCE-EMD Specialty Conference*, West Lafayette, Indiana.

Kelly, J.M. (1997), *Earthquake-Resistant Design with Rubber*, 2th Edition, Springer Verlag London Limited, UK.

Kelly, J.M. (1999), "The role of damping in seismic isolation", *Earthq. Eng. Struct. Dyn.*, **28**, 3-20.

Kiureghian, A.D. (1980), "Structural response to stationary excitation", *J. Eng. Mech. Div.*, **106**, 1195-1213.

Kiureghian, A.D. (1981), "A response spectrum method for random vibration analysis of MDF systems", *Earthq. Eng. Struct. Dyn.*, **9**, 419-435.

Narasimhan, S., Nagarajaiah, S., Johnson, E.A. and Gavin, H.P. (2006), "Smart base-isolated benchmark building. Part I: problem definition", *Struct. Control Hlth. Monit.*, **13**, 573-588.

Pekhan, G., Mander, J.B. and Chen, S.S. (1999), "Design and retrofit methodology for buildings structures with supplemental energy dissipation systems", Technical Report MCEER-99-0021; University of Buffalo.

Penzien, J. and Watabe, M. (1975), "Characteristics of 3-Dimensional earthquake ground motions", *Earthq. Eng. Struct. Dyn.*, **3**, 365-373.

Ramirez, O.M., Constantinou, M.C., Kircher, C.A., Whittaker, A.S., Johnson, M.W., Gómez, J.D. and Chrvsostomou, C.Z. (2000), "Development and evaluation of simplified procedures for analysis and design of buildings with passive energy dissipation systems", Technical Report MCEER-00-0010; University of Buffalo.

Sadek, F., Mohraz, B. and Riley, M.A. (1999), "Linear static and dynamic procedures for structures with velocity dependent supplemental dampers", NISTIR 6329; Buildings and Fire Research Laboratory, National Institute of Standards and Technology, Gaithersburg, MD.

Singh, M.P. (1980), "Seismic response by SRSS for non-proportional damping", *J. Eng. Mech. Div.*, ASCE, **106**(6), 1405-1419.

Sinha, R. and Igusa, T. (1995), "CQC and SRSS methods for non-classically damped structures", *Earthq. Eng. Struct. Dyn.*, **24**, 615-619.

Tsai, H. and Kelly, J.M. (1988), "Non-classical damping in dynamic analysis of base-isolated structures with internal

equipment", *Earthq. Eng. Struct. Dyn.*, **16**, 29-43.
Vanmarcke, E.H. (1972), "Properties of spectral moments with applications to random vibration", *J. Eng. Mech.*, **98**, 425-446.
Villaverde, R. (1988), "Rosenblueth's modal combination rule for systems with non-classical damping", *Earthq. Eng. Struct. Dyn.*, **16**, 315-328.
Warburton, G.B. and Soni, S.R. (1977), "Errors in response calculations for non-classically damped structures", *Earthq. Eng. Struct. Dyn.*, **5**(4), 365-377.
Yang, J.N., Sarkani, S. and Long, F.X. (1990), "A response spectrum approach for seismic analysis of non-classically damped structures", *Eng. Struct.*, **12**, 173-184.
Zhou, X.Y., Yu, R.F. and Dong, D. (2004), "Complex mode superposition algorithm for seismic responses of non-classically damped linear MDOF system", *J. Earthq. Eng.*, **8**(4), 597-641.

PL

Appendix A: Details of the influence matrices $\mathbf{R}_{s1}$, $\mathbf{R}_{s2}$ and $\mathbf{R}_{s3}$

In practice, a structural system is always modeled by a finite number of discrete members and lumped masses and for individual mass or node, there normally exist six DOFs (u_x, u_y, u_z, θ_x, θ_y, θ_z), i.e., three translations and three rotations, in the three-dimensional space. For isolated structures, the isolation slab is so rigid that all isolation bearings can deform uniformly, the isolation system can be modeled by an equivalent element at the center of mass of the base. The base, thus, has six DOFs, i.e., three horizontal displacements and three rotational displacements. The superstructure is subjected to the accelerations of the seismic input with three horizontal components and the base with six components. Therefore, their influence matrices, $\mathbf{R}_{s1}$ and $\mathbf{R}_{s2}$, have the following expressions

$$\mathbf{R}_{s1}=\begin{Bmatrix}\mathbf{r}_{s1}^{(1)}\\ \mathbf{r}_{s1}^{(2)}\\ \vdots\\ \mathbf{r}_{s1}^{(i)}\\ \vdots\\ \mathbf{r}_{s1}^{(N_s)}\end{Bmatrix} \qquad \mathbf{R}_{s2}=\begin{Bmatrix}\mathbf{r}_{s2}^{(1)}\\ \mathbf{r}_{s2}^{(2)}\\ \vdots\\ \mathbf{r}_{s2}^{(i)}\\ \vdots\\ \mathbf{r}_{s2}^{(N_s)}\end{Bmatrix} \tag{A.1}$$

where

$$\mathbf{r}_{s1}^{(i)}=\begin{bmatrix}1&0&0\\0&1&0\\0&0&1\\0&0&0\\0&0&0\\0&0&0\end{bmatrix} \quad \mathbf{r}_{s2}^{(i)}=\begin{bmatrix}1&0&0&0&e_z^{(i)}&-e_y^{(i)}\\0&1&0&-e_z^{(i)}&0&e_x^{(i)}\\0&0&1&e_y^{(i)}&-e_x^{(i)}&0\\0&0&0&1&0&0\\0&0&0&0&1&0\\0&0&0&0&0&1\end{bmatrix}$$

in $\mathbf{r}_{s2}^{(i)}$, $e_x^{(i)}$, $e_y^{(i)}$ and $e_z^{(i)}$ denote the distances to the *i*-th node from the center of mass of the base in *x*, *y* and *z* directions, respectively.

The base has only six DOFs and the influence matrix $\mathbf{R}_{s3}$ of the seismic excitation can be given by

$$\mathbf{R}_{s3}=\begin{bmatrix}1&0&0\\0&1&0\\0&0&1\\0&0&0\\0&0&0\\0&0&0\end{bmatrix} \tag{A.2}$$

As an instance, the benchmark isolated structure used in this paper consists of 9 levels and each level has two horizontal displacements and one rotational displacement about vertical axis per floor at the center of mass. The distances (m) to the center of mass of each floor from the bottom to the top from the center of mass of the base are

$\mathbf{e}_x=[-0.35,-0.32,0.11,0.16,0.16,0.16,0.16,0.16]$

$\mathbf{e}_y=[-1.42,-5.80,-7.20,-9.20,-9.20,-9.20,-9.20,-9.20]$

Thus, the influence matrices $\mathbf{R}_{s1}$ $\mathbf{R}_{s2}$ and $\mathbf{R}_{s3}$ can be obtained as

$$\mathbf{R}_{s1}=\begin{Bmatrix}\mathbf{r}_{s1}^{(1)}\\ \mathbf{r}_{s1}^{(2)}\\ \vdots\\ \mathbf{r}_{s1}^{(i)}\\ \vdots\\ \mathbf{r}_{s1}^{(8)}\end{Bmatrix}\quad \mathbf{R}_{s2}=\begin{Bmatrix}\mathbf{r}_{s2}^{(1)}\\ \mathbf{r}_{s2}^{(2)}\\ \vdots\\ \mathbf{r}_{s2}^{(i)}\\ \vdots\\ \mathbf{r}_{s2}^{(8)}\end{Bmatrix}\quad \mathbf{R}_{s3}=\begin{bmatrix}1&0&0\\0&1&0\\0&0&1\end{bmatrix}$$

where

$$\mathbf{r}_{s1}^{(i)}=\begin{bmatrix}1&0&0\\0&1&0\\0&0&1\end{bmatrix}\qquad \mathbf{r}_{s2}^{(i)}=\begin{bmatrix}1&0&-e_y^{(i)}\\0&1&e_x^{(i)}\\0&0&1\end{bmatrix}$$

Appendix B: Derivations of Eqs.(7)-(12)

For the convenience of description, the state equations are written here again, namely

$$\mathbf{A}\dot{\mathbf{v}}+\mathbf{B}\mathbf{v}=-\mathbf{E}\mathbf{T}\ddot{\mathbf{u}}_g \tag{B.1}$$

where

$$\mathbf{A}=\begin{bmatrix}\mathbf{0}&\mathbf{M}^*\\ \mathbf{M}^*&\mathbf{C}^*\end{bmatrix}\quad \mathbf{B}=\begin{bmatrix}-\mathbf{M}^*&\mathbf{0}\\ \mathbf{0}&\mathbf{K}^*\end{bmatrix}$$

$$\mathbf{E}=\begin{bmatrix}\mathbf{0}\\ \mathbf{R}^*\end{bmatrix}\qquad \mathbf{v}=\begin{Bmatrix}\dot{\mathbf{u}}^*\\ \mathbf{u}^*\end{Bmatrix}$$

Let λ be an admissible eigenvalue. Associated with each eigenvalue λ is an admissible eigenvector $\boldsymbol{\psi}$. The associated eigenvalue problem of Eq. (B.1) is given by

$$(\lambda\mathbf{A}+\mathbf{B})\boldsymbol{\psi}=\mathbf{0} \tag{B.2}$$

Since both **A** and **B** are non-positive definite matrices, eigenvalues λ_i and the relevant eigenvectors $\boldsymbol{\psi}_i$ are, in general, complex-valued and appear in conjugate pairs. The eigenvalue matrix (or spectral matrix), which is the assembly of all eigenvalues, is a diagonal matrix and denoted as

$$\boldsymbol{\Lambda}=\mathrm{diag}\begin{pmatrix}\lambda_1 & \bar{\lambda}_1 & \lambda_2 & \bar{\lambda}_2 & \cdots & \lambda_{Nc} & \bar{\lambda}_{Nc}\end{pmatrix} \tag{B.3}$$

The eigenvector matrix, which is the assembly of all eigenvectors, is denoted as

$$\boldsymbol{\Psi}=\begin{bmatrix}\boldsymbol{\psi}_1 & \bar{\boldsymbol{\psi}}_1 & \boldsymbol{\psi}_2 & \bar{\boldsymbol{\psi}}_2 & \cdots & \boldsymbol{\psi}_{Nc} & \bar{\boldsymbol{\psi}}_{Nc}\end{bmatrix} \tag{B.4}$$

In the eigenvector space, the state vector can be expressed as

$$\mathbf{v}(t)=\begin{Bmatrix}\dot{\mathbf{u}}^*(t)\\ \mathbf{u}^*(t)\end{Bmatrix}=\boldsymbol{\Psi}\mathbf{w}(t) \tag{B.5}$$

where

$\mathbf{w}(t)=[w_1(t),\bar{w}_1(t),w_2(t),\bar{w}_2(t),\cdots,w_{Nc}(t),\bar{w}_{Nc}(t)]^{\mathrm{T}}$ is the complex modal coordinate vector in the time domain.

Substituting Eq. (B.5) into Eq. (B.1) and pre-multiplying $\boldsymbol{\Psi}^{\mathrm{T}}$ to both sides of the resulting equation as well as making use of the orthogonality of the eigenvectors with respect to **A** and **B**, Eq. (B.1) can be transformed as

$$\begin{cases}\dot{w}_i(t)-\lambda_i w_i(t)=-\boldsymbol{\eta}_i\mathbf{T}\ddot{\mathbf{u}}_g(t)\\ \dot{\bar{w}}_i(t)-\bar{\lambda}_i\bar{w}_i(t)=-\bar{\boldsymbol{\eta}}_i\mathbf{T}\ddot{\mathbf{u}}_g(t)\end{cases}\quad i=1,2,\cdots,N_c \tag{B.6}$$

where $\boldsymbol{\eta}_i=\boldsymbol{\phi}_i^{\mathrm{T}}\mathbf{E}/(2\lambda_i\boldsymbol{\phi}_i^{\mathrm{T}}\mathbf{M}\boldsymbol{\phi}_i+\boldsymbol{\phi}_i^{\mathrm{T}}\mathbf{C}\boldsymbol{\phi}_i)$ denotes the modal participation factor. Hence, the vector $\mathbf{u}^*$ can be expressed as

$$\mathbf{u}^*(t)=\sum_{i=1}^{N_c}[\boldsymbol{\phi}_i\boldsymbol{\eta}_i\mathbf{T}\mathbf{z}_i(t)+\bar{\boldsymbol{\phi}}_i\bar{\boldsymbol{\eta}}_i\mathbf{T}\bar{\mathbf{z}}_i(t)] \tag{B.7}$$

if let

$$\dot{\mathbf{z}}_i(t)-\lambda_i\mathbf{z}_i(t)=-\ddot{\mathbf{u}}_g(t) \tag{B.8}$$

Applying the Laplace transform to Eqs. (B.7) and (B.8), respectively, yields

$$\mathbf{U}^*(s)=\sum_{i=1}^{N_c}[\boldsymbol{\phi}_i\boldsymbol{\eta}_i\mathbf{T}\mathbf{Z}_i(s)+\bar{\boldsymbol{\phi}}_i\bar{\boldsymbol{\eta}}_i\mathbf{T}\bar{\mathbf{Z}}_i(s)] \tag{B.9}$$

and

$$(s-\lambda_i)\mathbf{Z}_i(s)=-\ddot{\mathbf{U}}_g(s) \tag{B.10}$$

Substituting Eq. (B.10) into Eq. (B.9) yields

$$\begin{aligned}\mathbf{U}^*(s)&=-\left[\sum_{i=1}^{N_c}\left(\frac{\boldsymbol{\phi}_i\boldsymbol{\eta}_i}{s-\lambda_i}+\frac{\bar{\boldsymbol{\phi}}_i\bar{\boldsymbol{\eta}}_i}{s-\bar{\lambda}_i}\right)\right]\mathbf{T}\ddot{\mathbf{U}}_g(s)\\&=\left\{\sum_{i=1}^{N_c}\left[\boldsymbol{\rho}_i H_{\dot{q},i}(s)+\boldsymbol{\varphi}_i H_{q,i}(s)\right]\right\}\mathbf{T}\ddot{\mathbf{U}}_g(s)\end{aligned} \tag{B.11}$$

where $\boldsymbol{\rho}_i=2\,\mathrm{Re}(\boldsymbol{\phi}_i\boldsymbol{\eta}_i)$, $\boldsymbol{\varphi}_i=-2\,\mathrm{Re}(\bar{\lambda}_i\boldsymbol{\phi}_i\boldsymbol{\eta}_i)$ and

$$H_{\dot{q},i}(s)=-\frac{s}{s^2+2\xi_i\omega_i s+\omega_i^2}\quad H_{q,i}(s)=-\frac{1}{s^2+2\xi_i\omega_i s+\omega_i^2}$$

Taking the inverse Laplace transform of Eq. (B.11) leads to

$$\mathbf{u}^*(t)=\sum_{i=1}^{N_c}[\boldsymbol{\rho}_i\mathbf{T}\dot{\mathbf{q}}_i(t)+\boldsymbol{\varphi}_i\mathbf{T}\mathbf{q}_i(t)] \tag{B.12}$$

where $\dot{\mathbf{q}}_i(t)$ and $\mathbf{q}_i(t)$ are responses of the normalized SDOF system subjected to three-component seismic input , i.e.

$$\ddot{\mathbf{q}}_i(t)+2\xi_i\omega_i\dot{\mathbf{q}}_i(t)+\omega_i^2\mathbf{q}_i(t)=-\ddot{\mathbf{u}}_g(t) \tag{B.13}$$

Utilizing $\mathbf{u}_s=\boldsymbol{\Phi}_s\mathbf{y}_s$, the displacement vector of the isolated structure in the physical space can be obtained as

$$\begin{aligned}\mathbf{u}(t)&=\begin{Bmatrix}\mathbf{u}_s(t)\\ \mathbf{u}_b(t)\end{Bmatrix}=\begin{bmatrix}\boldsymbol{\Phi}_s&\\ &\mathbf{I}_{N_b}\end{bmatrix}\begin{Bmatrix}\mathbf{y}_s\\ \mathbf{u}_b\end{Bmatrix}\\&=\mathbf{T}'\mathbf{u}^*(t)=\sum_{i=1}^{N_c}\mathbf{T}'[\boldsymbol{\rho}_i\mathbf{T}\dot{\mathbf{q}}_i(t)+\boldsymbol{\varphi}_i\mathbf{T}\mathbf{q}_i(t)]\end{aligned} \tag{B.14}$$

where $\mathbf{T}'=\mathrm{diag}(\boldsymbol{\Phi}_s,\mathbf{I}_{N_b})$.